Journal of Glaciology

Article

Cite this article: Haris R, Chu W, Robel A (2024). What can radar-based measures of subglacial hydrology tell us about basal shear stress? A case study at Thwaites Glacier, West Antarctica. *Journal of Glaciology* **70**, e56, 1–9. https://doi.org/10.1017/jog.2024.3

Received: 28 August 2023
Revised: 17 December 2023
Accepted: 3 January 2024

Keywords:
ice-sheet modeling; radio-echo sounding; subglacial processes

Corresponding author:
Rohaiz Haris;
Email: rharis3@gatech.edu

cambridge.org/jog

What can radar-based measures of subglacial hydrology tell us about basal shear stress? A case study at Thwaites Glacier, West Antarctica

Rohaiz Haris, Winnie Chu and Alexander Robel

School of Earth and Atmospheric Sciences, Georgia Institute of Technology, Atlanta, GA USA

Abstract

Ice sheet models use observations to infer basal shear stress, but the variety of methods and datasets available has resulted in a wide range of estimates. Radar-based metrics such as reflectivity and specularity content have been used to characterize subglacial hydrologic conditions that are linked to spatial variations in basal shear stress. We explore whether radar metrics can be used to inform models about basal shear stress. At Thwaites Glacier, West Antarctica, we sample basal shear stress inversions across a wide range of ice sheet models to see how the basal shear stress distribution changes in regions of varying relative reflectivity and specularity content. Our results reveal three key findings: (1) Regions of high specularity content exhibit lower mean basal shear stresses (2) Wet and bumpy regions, as characterized by high relative reflectivity and low specularity content, exhibit higher mean basal shear stresses (3) Models disagree about what basal shear stress should be at the onset of rapid ice flow and high basal melt where relative reflectivity and specularity content are low.

1. Introduction

Glaciers and ice streams discharge ice from the interior of the Antarctic Ice Sheet to the ocean at a rate which is largely controlled by conditions at the ice-bed interface (Schoof, 2007). The influence of subglacial conditions on basal friction - and by extension on ice flow - is key to modeling the future potential evolution of the Antarctic ice sheet. Direct borehole observations over small areas of the ice sheet have been used to characterize the ice-bed interface by studying subglacial hydrologic systems (Hubbard and others, 1995) and basal friction (Pfeffer and others, 2000), but repeating these direct observations over the entire Antarctic Ice Sheet is logistically challenging. As such, alternative geophysical observational methods and forward models are typically used to analyze basal conditions over spatially extensive regions. Geophysical methods, such as seismic reflection (King, 2004) and radar sounding (Dowdeswell and Evans, 2004), are useful tools to indirectly characterize the ice-bed interface by inferring the locations of subglacial water (Chu and others, 2016), distribution of basal channels (Schroeder and others, 2013), and bed morphology (Smith, 1997). However, most individual geophysical surveys are limited to the local glacier scale and there are only a handful of repeated surveys (e.g., NASA Operation IceBridge) that cover larger areas of the Antarctic Ice Sheet.

Due to the lack of extensive physical observations on a catchment scale, basal shear stress is typically inferred from remote sensing observations (typically surface velocity and ice thickness) using control or data-assimilation methods (MacAyeal, 1993). However, the inferred basal shear stress is sensitively dependent on the details of the input dataset, the choice of the sliding law, the control method, and regularizations therein (Morlighem and others, 2010; Sergienko and Hindmarsh, 2013; Seroussi and others, 2013; Zhao and others, 2018). As a result, for the same area of an ice sheet, inversions can give a wide range of estimates for basal shear stress (Seroussi and others, 2020).

Inversions can be unstable, as a small amount of error or change in observations can lead to large differences in modeled parameters. Input observational datasets inherently have a small amount of error that can result in inversions trying to overfit the observations below the level of error in measurements. Furthermore, the transfer function relating variability in basal conditions to surface velocity or slope is a low-pass filter, resulting in surface properties responding to basal properties averaged over several ice thicknesses (Gudmundsson, 2003; Wolovick and others, 2023). As such, widely differing basal drag fields can reproduce similar surface velocities (Habermann and others, 2012) which makes inversions ill-posed when inferring basal shear stress from observations of surface velocities (Wolovick and others, 2023). Regularizations help to stabilize the inversion solution by imposing additional constraints that bias the solution and reduce overfitting. A common regularization method is the Tikhonov regularization, which determines how much weight to give to the cost function and can give preference to a solution with desirable properties (Habermann and others, 2012). To make an informed decision in choosing and adjusting regularization terms, it is therefore important to constrain bed characteristics, roughness, and subglacial hydrology.

Previous studies have characterized subglacial hydrology using other observable geophysical methods and investigated their relationship with basal friction. Kyrke-Smith and others (2017)

utilized seismic profiles to infer acoustic impedance in order to estimate mechanical basal conditions. Comparisons between the seismic observations and high resolution basal shear stress inversions show that there is a stronger correlation between acoustic impedance and basal slipperiness or basal drag at scales longer than the ice thickness (>7 km) compared to smaller scales. Other studies have used airborne radar sounding to infer characteristics and spatial variations of subglacial hydrology using bed reflectivity (i.e., brightness of bed echo returns) and specularity content (i.e., relative contribution of specular (mirror-like reflections) signals to the total returned bed energy) (Schroeder and others, 2013; Chu and others, 2021). Das and others (2023) conducted correlation experiments and found no strong correlation between relative reflectivity and the sliding-law parameter used to control basal friction in numerical ice sheet models. These studies have suggested a potential link between the spatial distribution of subglacial hydrology and basal shear stress based on geophysical observations. In this study, we examine the statistical relationship between radar metrics and basal shear stress in more detail by combining numerical ice sheet models and a high resolution radar sounding dataset from the Amundsen Sea Sector in West Antarctica. Our study site is Thwaites Glacier, located in the Amundsen Sea Embayment, which is a dominant contributor to Antarctic Ice Sheet mass loss (Pritchard and others, 2009).

2. Data and methods

2.1 Radar sounding observations

We use published radar bed reflectivity and specularity content observations from two airborne radar sounding studies to characterize subglacial hydrologic conditions at Thwaites Glacier (Schroeder and others, 2013; Chu and others, 2021). The radar metrics were calculated from radar sounding data measured by the High Capability Airborne Radar Sounder (HiCARS) system with a 60 MHz center frequency and 15 MHz bandwidth (Peters and others, 2007). The data was collected as part of a campaign that conducted airborne radar sounding surveys of the Amundsen Sea Embayment during the 2004/2005 austral field season (Holt and others, 2006; Vaughan and others, 2006).

Bed reflectivity describes the brightness of returned bed echoes and is mostly influenced by the difference in dielectric permittivity between two materials (Peters, 2005). A vertical transition between ice and liquid freshwater results in a 10–15 dB increase in reflectivity relative to the surrounding ice-bed interface (Peters, 2005; Chu and others, 2016; Young and others, 2016). Other material properties such as electrical conductivity can also impact reflectivity (Tulaczyk and Foley, 2020). We use relative reflectivity (relative to our study site as seen in Fig. 3b) from Chu and others (2021) which captures spatial variations within a study site as opposed to absolute reflectivity which is influenced by many unknown parameters specific to the site (Peters and others, 2007; Chu and others, 2021). We refer readers to Chu and others (2021) for more details of the reflectivity dataset used in our study.

Specularity content is a measure of the angular distribution of the bed echo power, with values ranging from 0 to 1 and is computed by finding the fraction of the total returned radar energy that is returned in a narrow angular distribution around the specular direction compared to energy diffusely scattered. We refer readers to Schroeder and others (2013) for more details of the specularity content dataset used in our study. Differences in ice-bedrock interface geometry produce unique scattering signatures that can be used to characterize interface roughness and subglacial hydrology. Thus, specularity content is typically interpreted to indicate a change in interface roughness (Schroeder and others, 2013). Smooth interfaces will return sharp mirror-like reflections. This results in higher specularity content values (>0.3) that are thought to be indicative of a smooth interface such as a region of low bed roughness or subglacial lakes with flat surfaces. Conversely, diffuse interfaces will scatter energy in all directions and have a low specularity content (<0.3) (Schroeder and others, 2013; Young and others, 2016; Chu and others, 2021).

The goal of our study is not to definitively distinguish between the influence of bed roughness versus material contrast on bed reflectivity or specularity content; but to explore whether these radar metrics correspond to any changes in basal shear stress suggested by ice sheet models. This is also the reason why we choose to combine both relative reflectivity and specularity content (each sensitive to a different degree to the presence of subglacial water or changes in bed roughness) to provide a more comprehensive interpretation of basal conditions at Thwaites Glacier.

2.2 Model-inferred basal friction

Basal shear stress on a continental scale is typically inferred from inverse methods in ice sheet models (MacAyeal, 1992; Sergienko and others, 2008; Pattyn and others, 2017) using large-scale remote sensing measurements such as ice velocity, surface elevation and ice thickness. We use previously published basal shear stress inversions from a subset of Antarctic ice sheet model simulations included in the most recent Ice Sheet Model Intercomparison project (Seroussi and others, 2020). We exclude models that have unphysical values of basal shear stress or low resolution over our study site. The subset of models include: AWI PISM1 (Bueler and Brown, 2009; Winkelmann and others, 2011; Aschwanden and others, 2012; Seroussi and others, 2020), JPL1 ISSM (Seroussi and others, 2020), PIK PISM1 (Bueler and Brown, 2009; Winkelmann and others, 2011; Seroussi and others, 2020), UCIJPL ISSM (Seroussi and others, 2020), UTAS ElmerIce (Seroussi and others, 2020), VUB AISMPALEO (Huybrechts, 1990, 2002; Seroussi and others, 2020), DOE MALI (Hoffman and others, 2018; Seroussi and others, 2020), NCAR CISM (Lipscomb and others, 2019; Seroussi and others, 2020). Each modeling group participating in ISMIP6 uses their own inversion method to initialize the basal sliding coefficient field, which is then held constant for the transient simulations of future ice sheet behavior which are the focus of the inter-comparison exercise. Thus, this ensemble of inversions is a representative sampling of the best estimates of basal shear stress which are used to predict future ice sheet behavior. We have also added the inversion from Sergienko and Hindmarsh (2013) which includes some finer resolution (kilometer-scale) features not present in ISMIP6 inversions.

Most inversions examined in this study use some variation of the control method described in MacAyeal (1993) to minimize the misfit between the observed and modeled ice sheet surface velocities (Morlighem and others, 2010). The control method uses a cost function and subsequent optimizations to reduce the error between a forward model's output and observations such as surface velocity or topography (Ranganathan and others, 2021). Different modeling groups use different variations of the cost function in MacAyeal (1993) and apply their own regularizations and optimizations as well. For example, some cost functions may prioritize reducing the velocity misfit in slow moving regions (Morlighem and others, 2010), while other cost functions may not consider velocity direction and only reduce misfit in the magnitude of velocities (Zhao and others, 2018). Other models use transient spin-up methods (Schoof, 2006; Pollard and DeConto, 2012) that assimilate observations to nudge the output to minimize the mismatch between modeled and observed data. Ultimately, such differences in inversion methodology and input data lead to

https://doi.org/10.1017/jog.2024.3 Published online by Cambridge University Press

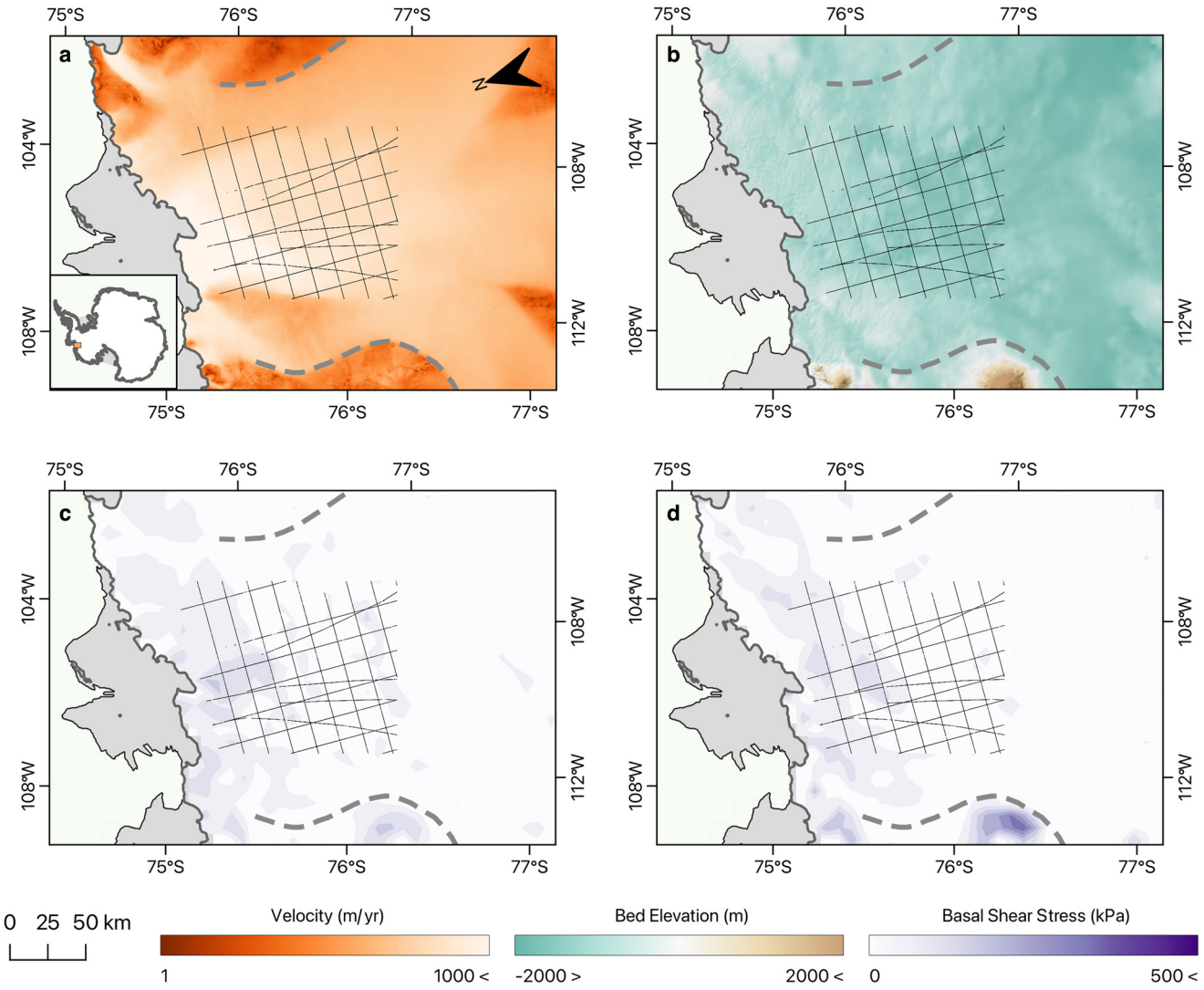

Figure 1. Site Map indicating radar flight tracks (black line) (Chu and others, 2021), shear margin (dotted gray line) (Schroeder and others, 2013), with (a) MEaSUREs ice velocity (Mouginot and others, 2017; Rignot and University Of California Irvine, 2017) using a logarithmic colorscale, (b) BedMachine v3 bed topography (Morlighem and others, 2020; Morlighem, 2022) & REMA hillshade (Howat and others, 2022), (c) NCAR CISM basal shear stress inversion (Lipscomb and others, 2019; Seroussi and others, 2020) and (d) JPL1 ISSM basal shear stress inversion (Seroussi and others, 2020).

a wide range of predicted basal shear stress among the models considered here. Since direct observations of basal shear stress are sparse (or absent entirely in some regions, including the region we consider in this study), inversions are not validated against observations. Thus, we instead consider a representative sample of nine inversions and analyze where these inversions agree and disagree with each other in terms of their statistical relationship to radar sounding metrics.

2.3 Statistical methods for comparison of radar observations and modeled data

Due to varying spatial resolutions of the basal shear stress inversions used in this study and the higher resolution of radar data, all inversions of basal shear stress are interpolated onto the radar flight track coordinates using linear interpolation. We only consider points where all inversions have estimates of basal shear stress to ensure a fair comparison across inversions.

Prior studies (e.g., Kyrke-Smith and others, 2017; Das and others, 2023) have attempted to quantify the relationship between measures of subglacial hydrology and basal shear stress using regression methods and generally failed to do so except at spatial scales larger than 7 km. The same is true for the radar and basal shear stress data used here. We first examined the linear regression between the modeled basal shear stress and the two radar indices, relative reflectivity and specularity content respectively. On a basin scale, the largest Pearson correlation coefficient observed across all models was -0.3269 between JPL1 ISSM basal shear stress and specularity content. While we observe a correlation between basal shear stress and radar metrics using the Pearson Correlation Coefficient, conducting statistical tests on large datasets can yield statistically significant results when there may be no practical relationship in reality (Johnson, 1999). The significance of the correlation between basal shear stress and radar metrics can be seen to be spurious as the regressions are heavily biased by the density of certain basal shear stress values in the dataset (Supplementary Figs. S2 & S3). In reality, basal shear stress has a very weak linear dependence on radar metrics. Instead, we use sampling statistics to determine if radar metrics can be used to classify regions with statistically significant variations in basal shear stress. After sub-sampling the model-based values of basal shear stress using various permutations of reflectivity and specularity content thresholds across the extent of the radar dataset, we analyze how the mean basal shear stress changes across different inversions and different radar metric thresholds. Basal shear stress samples with less than 100 values are not

https://doi.org/10.1017/jog.2024.3 Published online by Cambridge University Press

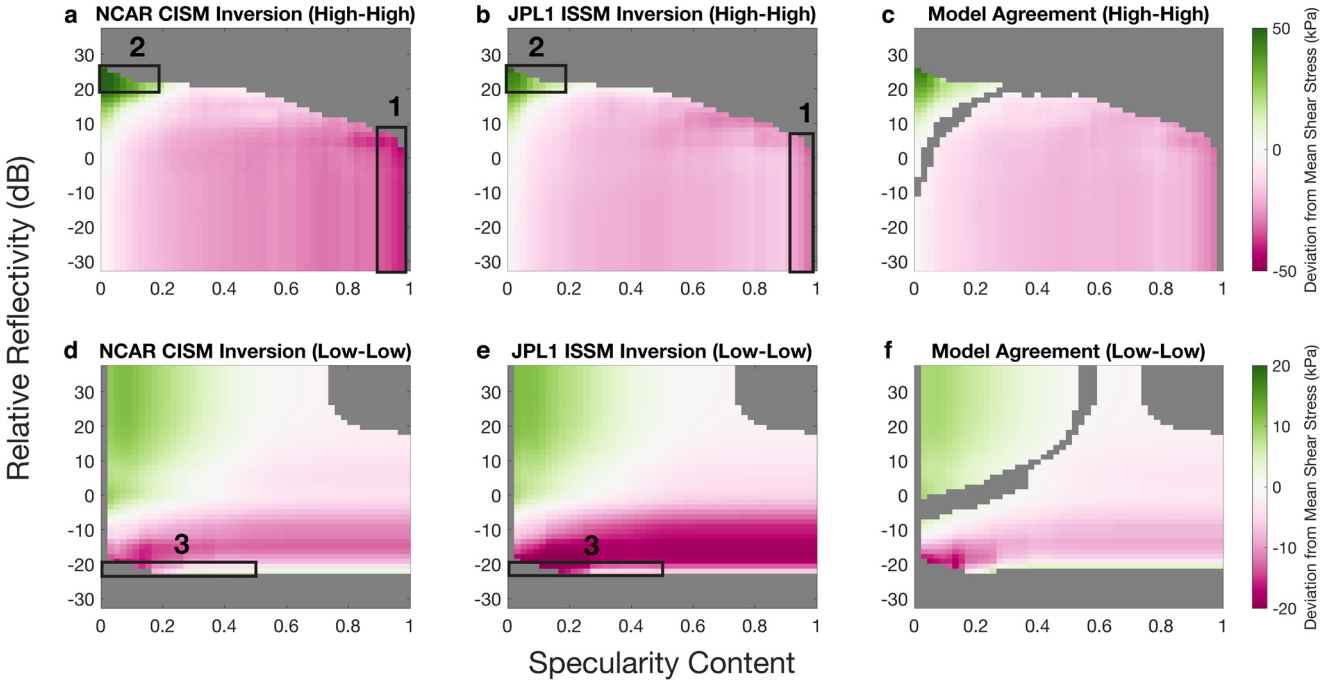

Figure 2. 2a and 2b show the high-high plots for NCAR CISM (Lipscomb and others, 2019; Seroussi and others, 2020) and JPL1 ISSM inversion (Seroussi and others, 2020) respectively. We apply thresholds when subsampling on the basis of radar data such that for a given grid cell in the figure, we subsample basal shear stress values that occur in regions of specularity content greater than X and relative reflectivity greater than Y where X and Y correspond to the x-axis and y-axis values for that grid cell respectively. 2d and 2e show the low-low plots for the NCAR CISM inversion and JPL1 ISSM inversion respectively. We apply thresholds when subsampling on the basis of radar data such that for a given grid cell in the figure, we subsample basal shear stress values that occur in regions of specularity content lower than X and relative reflectivity lower than Y where X and Y correspond to the x-axis and y-axis values for that grid cell respectively. The colormap for 2a, 2b, 2d & 2e represent the deviation in mean basal shear stress of the sample from the overall basal shear stress distribution. Grey areas represent NaN values where there are less than 100 values or more than 70% of the dataset. Regimes of significant deviation in mean basal shear stress are identified in 2a, 2b, 2d & 2e by numbers and corresponding rectangles. Figures 2c,f show where seven or more inversions agreed on the sign of deviation from mean basal shear stress on the high-high plot and low-low plot respectively. The colormap indicates the inter-model mean of the deviation in mean basal shear stress for that relative reflectivity and specularity threshold. Grey areas represent NaN values where there are less than 100 values or more than 70% of the dataset, or where seven or more inversions disagreed on the sign of deviation from mean basal shear stress.

considered to ensure that any changes in the basal shear stress distribution are not due to individual outliers within small sample sizes. We also identify where regions of significant deviation in mean basal shear stress occur and how they relate to other variables such as surface ice velocity (Figure 1a) and bed topography (Figure 1b).

Finally, we used two-sample Kolmogorov–Smirnov testing to verify whether sub-sampling basal shear stress on the basis of radar data produces a statistically significant difference in the sub-sampled basal shear stress distribution compared to randomly sampling the same number of points from the entire basal shear stress dataset. The two-sample Kolmogorov-Smirnov test (henceforth referred to as KS test) is a hypothesis test that evaluates the difference in cumulative distribution functions (CDFs) of two datasets and can be used to evaluate whether both samples share the same continuous distribution (Dimitrova and others, 2020). In KS testing, our null hypothesis is that the sub-sampled data and the overall basal shear stress data share the same distribution, which would indicate that reflectivity and specularity content are not useful tools for discriminating regions with different basal shear stress. Rejecting the null hypothesis for a particular reflectivity and specularity content threshold is a useful way to identify regions with different basal shear stresses. Samples that make up 70 percent or more of the inversion dataset are not considered as these are likely to be representative of the entire dataset and have well known issues when inferring the difference between distributions. The KS test is overly sensitive for large sample sizes and detects a statistically significant difference between the sub-sampled data and the complete basal shear stress dataset even if the actual difference is negligible (Sullivan and Feinn, 2012; Larson, 2018). Due to this sensitivity to sample size, we perform the KS test on data sub-sampled on the basis of reflectivity and specularity content and a random sample of the same size to avoid a Type I error which occurs when the null hypothesis is rejected incorrectly.

3. Results

We investigate whether using reflectivity and specularity content thresholds as sampling criteria produce statistically significant differences in basal shear stress across a range of model inversion products. The results from sub-sampling are illustrated in Figure 2 in a 50×50 grid, where each grid square reflects the deviation in mean basal shear stress for a sub-sample based on either maximum or minimum thresholds of specularity content and reflectivity, with respect to the mean basal shear stress over all radar flight lines.

Though we have calculated these basal shear stress deviations for all nine inversions considered in this study, Figures 2a,d plot results for the NCAR CISM inversion (Figure 1c) from ISMIP6 (Seroussi and others, 2020) and Figures 2b,e plot results of the JPL1 ISSM inversion (Figure 1d) from ISMIP6 (Seroussi and others, 2020). In Figures 2a,b, we apply a combination of reflectivity and specularity content thresholds to sub-sample each inversion such that for a given grid cell in the figure, we subsample basal shear stress values that occur in regions of specularity content greater than X and relative reflectivity greater than Y where X and Y correspond to the x-axis and y-axis values for that grid cell respectively. We refer to these plots as 'high-high' plots to indicate how the thresholds applied are 'Higher than specularity

https://doi.org/10.1017/jog.2024.3 Published online by Cambridge University Press

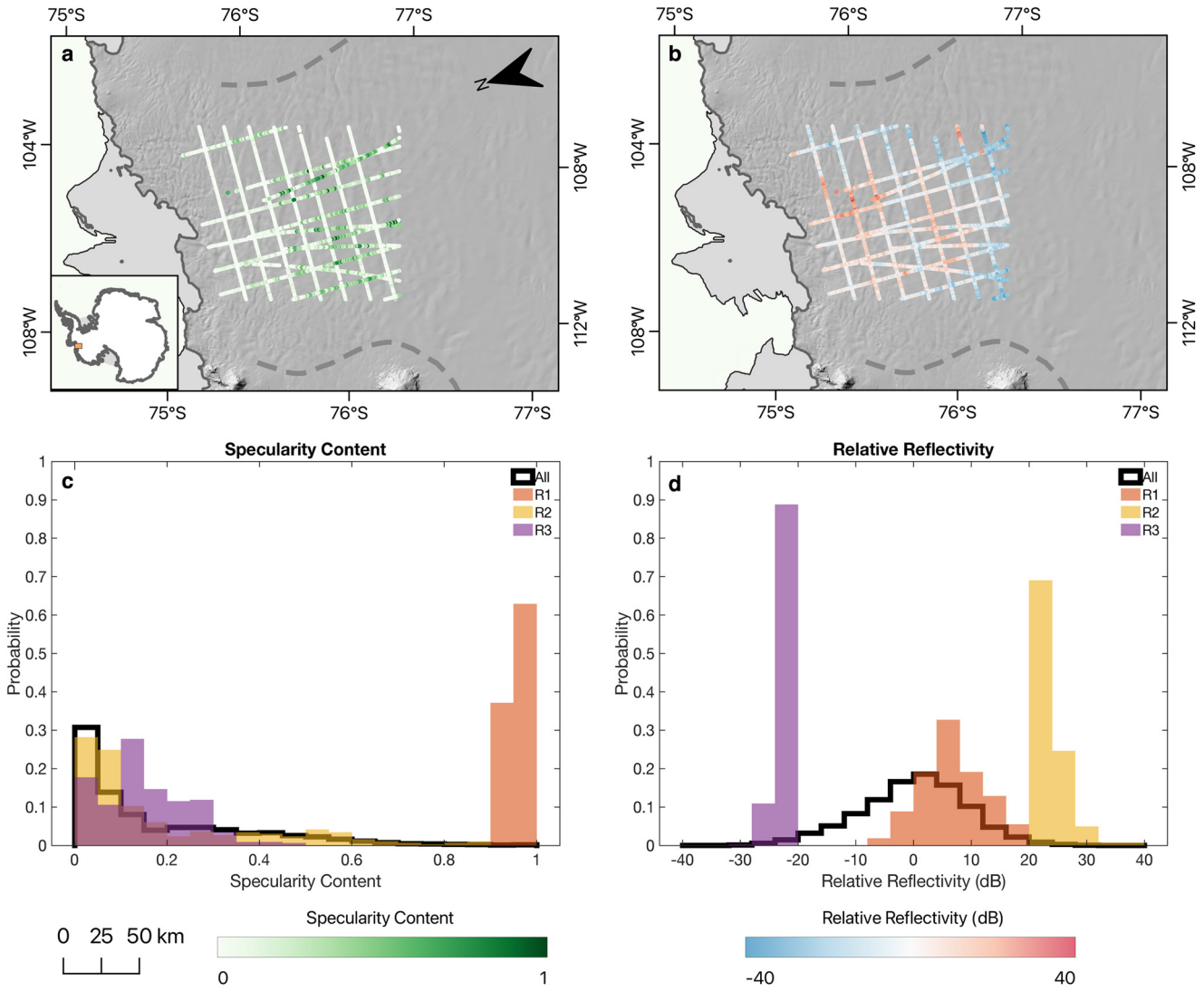

Figure 3. 3a and 3b plot the specularity content dataset (Schroeder and others, 2013) and relative reflectivity dataset (Chu and others, 2021) respectively with REMA hillshade (Howat and others, 2022) for our study site in Thwaites Glacier, West Antarctica. 3c and 3d plot histograms of specularity content and relative reflectivity respectively. In 3c and 3d, the histogram of the overall dataset is plotted with a thick black line while the histograms of the 3 regimes are plotted with colored bars and identified in the legend.

content-higher than relative reflectivity'. Conversely in Figures 2d, e (referred to as 'low-low' plots), the combination of reflectivity and specularity content thresholds applied for a given grid cell are specularity content less than X and relative reflectivity less than Y where X and Y correspond to the x-axis and y-axis values for that grid cell respectively. We refer to these plots as 'low-low' plots to indicate how the thresholds applied are 'lower than specularity content-lower than relative reflectivity'

We identify three regimes in Figures 2 and 3 where subsampling with reflectivity and specularity content thresholds lead to a substantial and coherent deviation in mean basal shear stress across most (or all nine) inversion products as verified by KS testing. While the range of spatial variation in basal shear stress differs between the models, the sign of deviation in mean basal shear stress is consistent across models for Regime 1 and Regime 2. Regime 1 occurs in areas where specularity content is >0.9, and there is a significant decrease in mean basal shear stress from 1 kPa up to 67 kPa depending on the inversion product. Regime 2 occurs in areas where relative reflectivity is between 20 dB and 35 dB and specularity content is typically <0.2 (though the exact reflectivity and specularity content boundaries vary depending on the inversion). In this bright but diffuse bed environment, there is a significant increase in mean basal shear stress from 4 kPa up to 126 kPa depending on the inversion product. Finally, regime 3 occurs in dim bed areas where relative reflectivity is <−20 dB and specularity content <0.5 where there is a significant deviation in mean basal shear stress across all inversions. However, inversions disagree on the sign of this deviation in mean basal shear stress. Three inversions indicate a significant increase in mean basal shear stress from 3 kPa up to 155 kPa depending to the inversion product. Conversely, the remaining six inversions indicate a significant decrease in mean basal shear stress from 2 kPa up to 21 kPa depending on the inversion product.

4. Discussion

In regions of high specularity content (Regime 1 identified in Fig. 2a,b and 3c,d), a lower mean basal shear stress was observed across all inversions. Reflected radar energy from smooth ice-bedrock interfaces is specular due to minimal scattering (Schroeder and others, 2015; Young and others, 2016). Regions of high specularity content have also been proposed as the location of broad canals incised into the subglacial till below Thwaites Glacier (Schroeder and others, 2013) or spatially continuous subglacial water sheets, which are both thought to reduce

https://doi.org/10.1017/jog.2024.3 Published online by Cambridge University Press

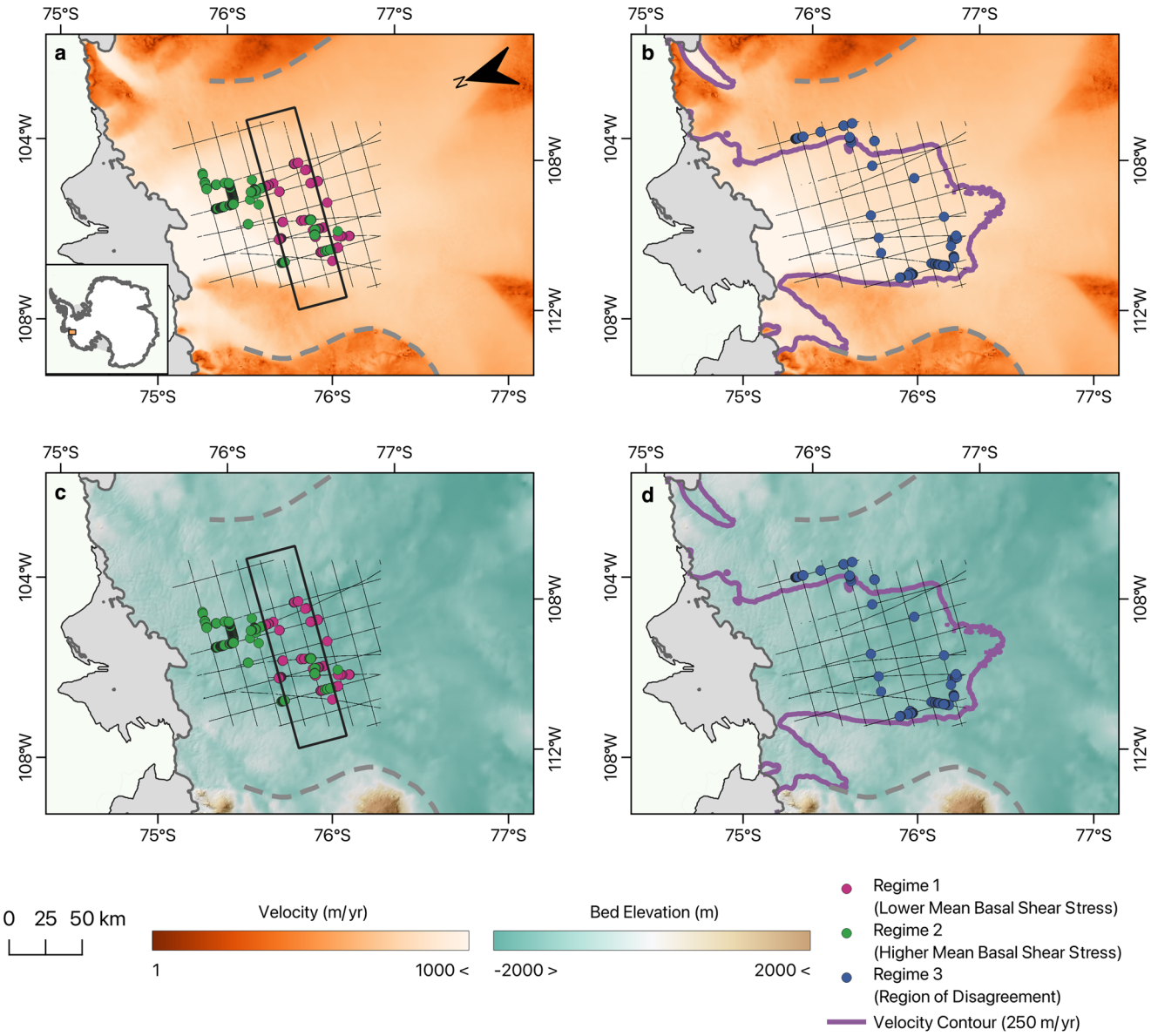

Figure 4. Spatial plot to observe variations in regions of significant deviation in mean basal shear stress. (a) Regime 1 where there is high specularity content (pink scatter markers showing lower mean basal shear stress) and Regime 2 where there is high reflectivity and low specularity content (green scatter markers showing higher mean basal shear stress) with MEaSUREs ice velocity plotted with a logarithmic colorscale (Mouginot and others, 2017; Rignot and University Of California Irvine, 2017), (b) Regime 3 where there is low reflectivity and low specularity (blue scatter markers indicating disagreement between models on what basal shear stress should be) with MEaSUREs ice velocity plotted with a logarithmic colorscale. (c) Regime 1 and Regime 2 with BedMachine v3 bed topography (Morlighem and others, 2020; Morlighem, 2022) and REMA hillshade (Howat and others, 2022), (d) Regime 3 with BedMachine v3 bed topography and REMA hillshade. The box in (a) and (c) represents our identified transition from a distributed to channelized system accompanied by an increase in mean basal shear stress. The purple contour line in (b) and (d) represents where ice velocity is 250 m yr^{-1}.

basal friction over large regions (Walder and Fowler, 1994; Creyts and Schoof, 2009).

Regions of low specularity content and high reflectivity (Regime 2 identified in Figs. 2a,b and 3c,d) show a higher mean basal shear stress across all inversions. The combination of low specularity content and high reflectivity is thought to be indicative of wet regions with a rough ice surface, which would be seen in concentrated Röthlisberger channels of water incised upward into the basal glacier ice (Schroeder and others, 2013). Such concentrated channels reduce the water flow through extensive distributed drainage systems, and so are thought to increase basal friction on average (Schoof, 2010), which is consistent with our findings of higher mean basal shear stress in these regions.

Regions of high specularity content and lower mean basal shear stress are located in the upstream reaches of the Thwaites catchment, while regions of low specularity content, high reflectivity and higher mean basal shear stress are mostly located in the downstream reaches of the Thwaites catchment. It has been theorized that the transition from a distributed to channelized water system at Thwaites Glacier is accompanied by an increase in basal shear stress (Schroeder and others, 2013). Our results are consistent with this prior hypothesis where we see an increase in mean basal shear stress from Regime 1 to Regime 2. We independently identify this transition in Figures 4a,c which is consistent with the transition identified in Schroeder and others (2013).

Regions of low reflectivity and low specularity content (Regime 3 identified in Figs. 2d,e and 3c,d) are indicative of a dry bed and show strong deviations from mean basal shear stress over the whole Thwaites study within particular inversions, but the sign of the deviation is not consistent between inversions. Three inversions considered in this study have high basal shear stress in low reflectivity and low specularity content regions, while the other six inversions have low basal shear stress. This region of disagreement between inversions is occurring at the onset of rapid ice flow and

https://doi.org/10.1017/jog.2024.3 Published online by Cambridge University Press

high basal melt (i.e., where ice velocity is approximately 250 m yr^{-1} in Figs. 4b,d denoted by the purple contour). The location of onset of rapid flow is known to vary widely between models due to generally inadequate treatments of the thermo-mechanical conditions in ice stream onset regions (Mantelli and Schoof, 2019; Mantelli and others, 2019). Models taking part in ISMIP6 may also differ on the location of streaming ice flow due to differing horizontal resolution or ice flow approximations (Payne and others, 2000; Hindmarsh, 2009). We thus identify a distinct radar signature of low reflectivity and low specularity content (Regime 3 in Figs. 3c,d) for the location of onset rapid ice flow where models disagree on the sign of deviation in mean basal shear stress.

We also identify two additional regimes of deviation in mean basal shear stress that is observed across all models; a regime of low specularity (green arm of the 'L' found in Figs. 2d,e) and a regime of low reflectivity (red arm of the 'L' found in Figs. 2d,e). A large fraction of the overall dataset is located in these two regimes. As a result, we do not focus our analysis on these regimes as they do not provide a useful criteria for sub-sampling basal shear stress inversions.

Other studies have also investigated the correspondence between indirect geophysical measures of subglacial hydrology to basal shear stress. Das and others (2023) calculated correlations between radar reflectivity and sliding law parameter (representative of basal friction) for three models and were unable to find a strong correlation. Kyrke-Smith and others (2017) found that there may not be a discernible relationship between subglacial hydrology and basal shear stress at short length scales (below 7 km), as they observed no correlation between acoustic impedance and basal shear stress within seismic profiles. However, a stronger correlation was observed when values were averaged over an ice thickness scale and distinct profiles were compared. Our study is consistent with the conclusions of Das and others (2023) and Kyrke-Smith and others (2017). We were unable to find a statistically significant relationship between basal shear stress and reflectivity or specularity content using regression techniques across radar profiles.

However, we do identify at least two useful radar metric thresholds for identifying regions of substantial deviations in basal shear stress which are statistically distinct from random sampling of basal shear stress data. This novel approach has also revealed that regions of low relative reflectivity and low specularity content indicative of a dry bed consistently occur at the zone of Thwaites Glacier where ice starts to flow fast. However, basal shear stress inversions tend to disagree about the basal shear stress in this region, thus requiring better constraints to be able to model ice flow in this region more accurately. The relationship between subglacial hydrology and basal shear stress may not be apparent at short length scales which are filtered out by ice sheet dynamics (Raymond and Gudmundsson, 2005) and may not be apparent in surface velocity which is the main constraint for basal shear stress inversions. Many sliding laws quantify the relationships between ice velocity, basal shear stress and basal water pressure. However, other factors may also play a role in controlling basal sliding, and radar sounding provides independent constraints on those factors that may not be captured by current inversion methods.

5. Conclusion

Different ice sheet models use different methods and datasets to estimate basal shear stress. In this study, we have shown that there are broad relationships between basal shear stress as determined by velocity inversions and radar metrics across models and locations within our study site at Thwaites Glacier, West Antarctica. We also use radar sounding to identify regions of low relative reflectivity and low specularity content characterized by a unique radar signature where models produce widely differing constraints on basal shear stress.

Presently, ice velocity and thickness are the main constraints for inversions. The results of this study indicate that radar sounding can potentially provide an independent constraint on subglacial properties that have been previously theorized to influence basal shear stress. However, ground-truth constraints from borehole measurements of basal shear stress or other methods are necessary since the relationships identified in this study are themselves based on existing inversions. We also find that reflectivity and specularity content contain spatial variations that cannot be explained by current basal shear stress estimates derived from ice velocity alone, thus indicating that they may contain additional information that could be valuable to models, e.g., using subglacial hydrology models. Constraints based on thresholds in radar metric data could be incorporated into control methods using inequality constraints, for which there are existing optimization methods (Bryson and others, 1963). While results from this study have shown that radar can be useful in providing constrains on factors not yet captured by inversions, further work on data assimilation into ice sheet models is required before radar sounding metrics can be used directly to inform ice-flow models on subglacial conditions.

Supplementary material. The supplementary material for this article can be found at https://doi.org/10.1017/jog.2024.3

Data. The code used in this study can be found on Github (https://github.com/rohaizharis/inversion_radar2022). The bed reflectivity data is from Chu and others (2021) and specularity content data is from Schroeder and others (2013). The processed radargrams and derived parameters from Chu and others (2021) can be found on the USAP-DC (https://doi.org/10.15784/601436). The inversions used in this study are from Sergienko and Hindmarsh (2013) and Seroussi and others (2020). The interpolated data for use with the code can be found on Zenodo (https://doi.org/10.5281/zenodo.10391022). The surface ice velocity from MEaSUREs (Rignot and University Of California Irvine, 2017; Mouginot and others, 2017), bed topography from BedMachine v3 (Morlighem and others, 2020; Morlighem, 2022), surface elevation hillshade from REMA (Howat and others, 2022), can be found online.

Acknowledgements. All authors were supported using startup funds from Georgia Institute of Technology. We would like to thank Vincent Verjans, Ziad Rashed, Angelo Tarzona and Kiera Tran for their feedback on the figures shown. We would also like to thank editor Dustin Schroeder and two anonymous reviewers for their constructive feedback that helped to improve the manuscript.

References

Aschwanden A, Bueler E, Khroulev C and Blatter H (2012) An enthalpy formulation for glaciers and ice sheets. *Journal of Glaciology* **58**(209), 441–457. doi: 10.3189/2012JoG11J088

Bryson AE, Denham WF and Dreyfus SE (1963) Optimal programming problems with inequality constraints. *AIAA Journal* **1**(11), 2544–2550. doi: 10.2514/3.2107

Bueler E and Brown J (2009) Shallow shelf approximation as a 'sliding law' in a thermomechanically coupled ice sheet model. *Journal of Geophysical Research: Earth Surface* **114**(F3), 2008JF001179. doi: 10.1029/2008JF001179

Chu W and 5 others (2016) Extensive winter subglacial water storage beneath the Greenland Ice Sheet. *Geophysical Research Letters* **43**(24), 12484–12492. doi: 10.1002/2016GL071538

Chu W and 8 others (2021) Multisystem synthesis of radar sounding observations of the Amundsen sea sector from the 2004–2005 field season. *Journal of Geophysical Research: Earth Surface* **126**(10), 1–17. doi: 10.1029/2021JF006296

Creyts TT and Schoof CG (2009) Drainage through subglacial water sheets. *Journal of Geophysical Research* **114**(F4), F04008. doi: 10.1029/2008JF001215

Das I and 5 others (2023) In the quest of a parametric relation between ice sheet model inferred Weertman's sliding–law parameter and airborne radar–derived basal reflectivity underneath Thwaites glacier, Antarctica. *Geophysical Research Letters* **50**(10), e2022GL098910. doi: 10.1029/2022GL098910

Dimitrova DS, Kaishev VK and Tan S (2020) Computing the Kolmogorov–Smirnov distribution when the underlying CDF is purely discrete, mixed, or continuous. *Journal of Statistical Software* **95**(10), 1–42. doi: 10.18637/jss.v095.i10

Dowdeswell JA and Evans S (2004) Investigations of the form and flow of ice sheets and glaciers using radio-echo sounding. *Reports on Progress in Physics* **67**(10), 1821–1861. doi: 10.1088/0034-4885/67/10/R03

Gudmundsson GH (2003) Transmission of basal variability to a glacier surface. *Journal of Geophysical Research: Solid Earth* **108**(B5), 2002JB002107. doi: 10.1029/2002JB002107

Habermann M, Maxwell D and Truffer M (2012) Reconstruction of basal properties in ice sheets using iterative inverse methods. *Journal of Glaciology* **58**(210), 795–808. doi: 10.3189/2012JoG11J168

Hindmarsh RCA (2009) Consistent generation of ice-streams via thermo-viscous instabilities modulated by membrane stresses. *Geophysical Research Letters* **36**(6), L06502. doi: 10.1029/2008GL036877

Hoffman MJ and 9 others (2018) MPAS-Albany Land Ice (MALI): a variable-resolution ice sheet model for Earth system modeling using Voronoi grids. *Geoscientific Model Development* **11**(9), 3747–3780. doi: 10.5194/gmd-11-3747-2018

Holt JW and 8 others (2006) New boundary conditions for the West Antarctic ice sheet: Subglacial topography of the Thwaites and Smith glacier catchments. *Geophysical Research Letters* **33**(9), L09502. doi: 10.1029/2005GL025561

Howat I and 17 others (2022) The Reference Elevation Model of Antarctica - Mosaics, Version 2 (doi: 10.7910/DVN/EBW8UC).

Hubbard BP, Sharp MJ, Willis IC, Nielsen MK and Smart CC (1995) Borehole water-level variations and the structure of the subglacial hydrological system of Haut Glacier d'Arolla, Valais, Switzerland. *Journal of Glaciology* **41**(139), 572–583. doi: 10.3189/S0022143000034894

Huybrechts P (1990) A 3-D model for the Antarctic ice sheet: a sensitivity study on the glacial-interglacial contrast. *Climate Dynamics* **5**(2), 79–92. doi: 10.1007/BF00207423

Huybrechts P (2002) Sea-level changes at the LGM from ice-dynamic reconstructions of the Greenland and Antarctic ice sheets during the glacial cycles. *Quaternary Science Reviews* **21**(1–3), 203–231. doi: 10.1016/S0277-3791(01)00082-8

Johnson DH (1999) The insignificance of statistical significance testing. *The Journal of Wildlife Management* **63**(3), 763. doi: 10.2307/3802789

King EC (2004) Seismic evidence for a water-filled canal in deforming till beneath Rutford Ice Stream, West Antarctica. *Geophysical Research Letters* **31**(20), L20401. doi: 10.1029/2004GL020379

Kyrke-Smith TM, Gudmundsson GH and Farrell PE (2017) Can seismic observations of bed conditions on ice streams help constrain parameters in ice flow models?: comparison of inversions and seismics. *Journal of Geophysical Research: Earth Surface* **122**(11), 2269–2282. doi: 10.1002/2017JF004373

Larson LG (2018) *Investigating statistical vs. practical significance of the Kolmogorov–Smirnov two-sample test using power simulations and resampling procedures*. Ph.D. thesis.

Lipscomb WH and 14 others (2019) Description and evaluation of the community ice sheet model (CISM) v2.1. *Geoscientific Model Development* **12**(1), 387–424. doi: 10.5194/gmd-12-387-2019

MacAyeal DR (1992) The basal stress distribution of ice stream E, Antarctica, inferred by control methods. *Journal of Geophysical Research* **97**(B1), 595. doi: 10.1029/91JB02454

MacAyeal DR (1993) A tutorial on the use of control methods in ice-sheet modeling. *Journal of Glaciology* **39**(131), 91–98. doi: 10.3189/S0022143000015744

Mantelli E and Schoof C (2019) Ice sheet flow with thermally activated sliding. Part 2: the stability of subtemperate regions. *Proceedings of the Royal Society A: Mathematical, Physical and Engineering Sciences* **475**(2231), 20190411. doi: 10.1098/rspa.2019.0411

Mantelli E, Haseloff M and Schoof C (2019) Ice sheet flow with thermally activated sliding. Part 1: the role of advection. *Proceedings of the Royal Society A: Mathematical, Physical and Engineering Sciences* **475**(2230), 20190410. doi: 10.1098/rspa.2019.0410

Morlighem M (2022) MEaSUREs BedMachine Antarctica, Version 3.

Morlighem M and 5 others (2010) Spatial patterns of basal drag inferred using control methods from a full-Stokes and simpler models for Pine Island Glacier, West Antarctica: SPATIAL PATTERNS OF BASAL DRAG. *Geophysical Research Letters* **37**(14), 1–6. doi: 10.1029/2010GL043853

Morlighem M and 36 others (2020) Deep glacial troughs and stabilizing ridges unveiled beneath the margins of the Antarctic ice sheet. *Nature Geoscience* **13**(2), 132–137. doi: 10.1038/s41561-019-0510-8

Mouginot J, Rignot E, Scheuchl B and Millan R (2017) Comprehensive annual ice sheet velocity mapping using landsat-8, Sentinel-1, and RADARSAT-2 Data. *Remote Sensing* **9**(4), 364. doi: 10.3390/rs9040364

Pattyn F, Favier L, Sun S and Durand G (2017) Progress in numerical modeling of Antarctic ice-sheet dynamics. *Current Climate Change Reports* **3**(3), 174–184. doi: 10.1007/s40641-017-0069-7

Payne AJ and 10 others (2000) Results from the EISMINT model intercomparison: the effects of thermomechanical coupling. *Journal of Glaciology* **46**(153), 227–238. doi: 10.3189/172756500781832891

Peters M and 5 others (2007) Along-track focusing of airborne radar sounding data from West Antarctica for improving basal reflection analysis and layer detection. *IEEE Transactions on Geoscience and Remote Sensing* **45**(9), 2725–2736. doi: 10.1109/TGRS.2007.897416

Peters ME (2005) Analysis techniques for coherent airborne radar sounding: application to West Antarctic ice streams. *Journal of Geophysical Research* **110**(B6), B06303. doi: 10.1029/2004JB003222

Pfeffer WT, Humphrey NF, Amadei B, Harper J and Wegmann J (2000) In situ stress tensor measured in an Alaskan glacier. *Annals of Glaciology* **31**, 229–235. doi: 10.3189/172756400781820354

Pollard D and DeConto RM (2012) A simple inverse method for the distribution of basal sliding coefficients under ice sheets, applied to Antarctica. *The Cryosphere* **6**(5), 953–971. doi: 10.5194/tc-6-953-2012

Pritchard HD, Arthern RJ, Vaughan DG and Edwards LA (2009) Extensive dynamic thinning on the margins of the Greenland and Antarctic ice sheets. *Nature* **461**(7266), 971–975. doi: 10.1038/nature08471

Ranganathan M, Minchew B, Meyer CR and Gudmundsson GH (2021) A new approach to inferring basal drag and ice rheology in ice streams, with applications to West Antarctic Ice Streams. *Journal of Glaciology* **67**(262), 229–242. doi: 10.1017/jog.2020.95

Raymond MJ and Gudmundsson GH (2005) On the relationship between surface and basal properties on glaciers, ice sheets, and ice streams. *Journal of Geophysical Research* **110**(B8), B08411. doi: 10.1029/2005JB003681

Rignot E and University Of California Irvine (2017) MEaSUREs Annual Antarctic Ice Velocity Maps, 2006-2017, Version 1.

Schoof C (2006) Variational methods for glacier flow over plastic till. *Journal of Fluid Mechanics* **555**, 299. doi: 10.1017/S0022112006009104

Schoof C (2007) Ice sheet grounding line dynamics: Steady states, stability, and hysteresis. *Journal of Geophysical Research* **112**(F3), F03S28. doi: 10.1029/2006JF000664

Schoof C (2010) Ice-sheet acceleration driven by melt supply variability. *Nature* **468**(7325), 803–806. doi: 10.1038/nature09618

Schroeder DM, Blankenship DD and Young DA (2013) Evidence for a water system transition beneath Thwaites Glacier, West Antarctica. *Proceedings of the National Academy of Sciences* **110**(30), 12225–12228. doi: 10.1073/pnas.1302828110

Schroeder DM, Blankenship DD, Raney RK and Grima C (2015) Estimating subglacial water geometry using radar bed echo specularity: application to Thwaites glacier, West Antarctica. *IEEE Geoscience and Remote Sensing Letters* **12**(3), 443–447. doi: 10.1109/LGRS.2014.2337878

Sergienko OV and Hindmarsh RCA (2013) Regular patterns in frictional resistance of ice-stream beds seen by surface data inversion. *Science* **342**(6162), 1086–1089. doi: 10.1126/science.1243903

Sergienko OV, Bindschadler RA, Vornberger PL and MacAyeal DR (2008) Ice stream basal conditions from block-wise surface data inversion and simple regression models of ice stream flow: Application to Bindschadler Ice Stream. *Journal of Geophysical Research* **113**(F4), F04010. doi: 10.1029/2008JF001004

Seroussi H and 5 others (2013) Dependence of century-scale projections of the Greenland ice sheet on its thermal regime. *Journal of Glaciology* **59**(218), 1024–1034. doi: 10.3189/2013JoG13J054

Seroussi H and 46 others (2020) ISMIP6 Antarctica: a multi-model ensemble of the Antarctic ice sheet evolution over the 21st century. *The Cryosphere* **14**(9), 3033–3070. doi: 10.5194/tc-14-3033-2020

Smith AM (1997) Basal conditions on Rutford ice stream, West Antarctica, from seismic observations. *Journal of Geophysical Research: Solid Earth* **102**(B1), 543–552. doi: 10.1029/96JB02933

Sullivan GM and Feinn R (2012) Using effect size–or why the P value is not enough. *Journal of Graduate Medical Education* **4**(3), 279–282. doi: 10.4300/JGME-D-12-00156.1

https://doi.org/10.1017/jog.2024.3 Published online by Cambridge University Press

Tulaczyk SM and Foley NT (2020) The role of electrical conductivity in radar wave reflection from glacier beds. *The Cryosphere* **14**(12), 4495–4506. doi: 10.5194/tc-14-4495-2020

Vaughan DG and 9 others (2006) New boundary conditions for the West Antarctic ice sheet: subglacial topography beneath pine Island Glacier. *Geophysical Research Letters* **33**(9), L09501. doi: 10.1029/2005GL025588

Walder JS and Fowler A (1994) Channelized subglacial drainage over a deformable bed. *Journal of Glaciology* **40**(134), 3–15. doi: 10.3189/S0022143000003750

Winkelmann R and 6 others (2011) The potsdam parallel ice sheet model (PISM-PIK)–part 1: model description. *The Cryosphere* **5**(3), 715–726. doi: 10.5194/tc-5-715-2011

Wolovick M, Humbert A, Kleiner T and Rückamp M (2023) Regularization and L-curves in ice sheet inverse models: a case study in the Filchner–Ronne catchment. *The Cryosphere* **17**(12), 5027–5060. doi: 10.5194/tc-17-5027-2023

Young DA, Schroeder DM, Blankenship DD, Kempf SD and Quartini E (2016) The distribution of basal water between Antarctic subglacial lakes from radar sounding. *Philosophical Transactions of the Royal Society A: Mathematical, Physical and Engineering Sciences* **374**(2059), 20140297. doi: 10.1098/rsta.2014.0297

Zhao C and 5 others (2018) Basal friction of Fleming glacier, Antarctica – part 1: sensitivity of inversion to temperature and bedrock uncertainty. *The Cryosphere* **12**(8), 2637–2652. doi: 10.5194/tc-12-2637-2018

https://doi.org/10.1017/jog.2024.3 Published online by Cambridge University Press